Steel and Composite Structures, *Vol. 28, No. 5 (2018) 541-557*
DOI: https://doi.org/10.12989/scs.2018.28.5.541

Vibration analysis of sandwich sectorial plates considering FG wavy CNT-reinforced face sheets

Vahid Tahouneh*

Young Researchers and Elite Club, *Islamshahr Branch*, *Islamic Azad University*, *Islamshahr*, *Iran*

(*Received December 8, 2017, Revised May 18, 2018, Accepted June 27, 2018*)

Abstract. This paper presents the influence of carbon nanotubes (CNTs) waviness and aspect ratio on the vibrational behavior of functionally graded nanocomposite sandwich annular sector plates resting on two-parameter elastic foundations. The carbon nanotube-reinforced (CNTR) sandwich plate has smooth variation of CNT fraction along the thickness direction. The distributions of CNTs are considered functionally graded (FG) or uniform along the thickness and their mechanical properties are estimated by an extended rule of mixture. In this study, the classical theory concerning the mechanical efficiency of a matrix embedding finite length fibers has been modified by introducing the tube-to-tube random contact, which explicitly accounts for the progressive reduction of the tubes' effective aspect ratio as the filler content increases. Effects of CNT distribution, volume fraction, aspect ratio and waviness, and also effects of Pasternak's elastic foundation coefficients, sandwich plate thickness, face sheets thickness and plate aspect ratio are investigated on the free vibration of the sandwich plates with wavy CNT-reinforced face sheets. The study is carried out based on three-dimensional theory of elasticity and in contrary to two-dimensional theories, such as classical, the first- and the higher-order shear deformation plate theories, this approach does not neglect transverse normal deformations. The sandwich annular sector plate is assumed to be simply supported in the radial edges while any arbitrary boundary conditions are applied to the other two circular edges including simply supported, clamped and free.

Keywords: CNTs waviness and aspect ratio; sandwich structures; vibration; rule of mixture; two-parameter elastic foundations; functionally graded materials; sectorial plates

1. Introduction

Normally, functionally graded materials (FGMs) are heterogeneous materials in which the elastic and thermal properties change from one surface to the other, gradually and continuously. The material is constructed by smoothly changing the volume fraction of its constituent materials. FGMs offer great promise in applications where the operating conditions are severe, including spacecraft heat shields, heat exchanger tubes, plasma facings for fusion reactors, engine components, and high-power electrical contacts or even magnets. For example, in a conventional thermal barrier coating for high-temperature applications, a discrete layer of ceramic material is bonded to a metallic structure. However, the abrupt transition in material properties across the interface between distinct materials can cause large interlaminar stresses and lead to plastic deformation or cracking (Finot and Suresh 1996). These adverse effects can be alleviated by functionally grading the material to have a smooth spatial variation of material composition. The concept of FGMs was first introduced in Japan in 1984. Since then it has gained considerable attention (Koizumi 1993). A lot of different applications of FGMs can be found in (Zhu and Meng 1995). Owing to the superior properties against the conventional composite laminates, FGMs have found increasing applications in modern engineering designs, such as aircraft fuselage, rocking-motor casing, packaging materials in microelectronic industry, human implants, and so on. FG sectorial plates have extensive applications in different engineering branches. For mechanical engineering and aerospace engineering it can be used in different aircraft components such as turbine or fan blades and also vacuum filter segment with replaceable sector plates. In civil engineering, this kind of structure has many practical applications for curved bridge decks.

Ramakris and Kunukkas (1973) provided a closed-form analytical solution for free vibration of an annular sector plate with radial edges simply supported. Mukhopadhyay (1979, 1982) used a semi-analytical method and Srinivasan and Thiruvenkatachari (1983, 1986) used the integral equation technique to analyze the vibrations of annular sector plates, respectively. Kim and Dickinson (1989) used one-dimensional (1-D) orthogonal polynomials and Liew and Lam (1993) used two-dimensional orthogonal polynomials as admissible functions to study the free vibration of annular sector plates by the Rayleigh-Ritz method. Ramaiah and Vijayakumar (1974) studied the free vibration of annular sector plates with simply supported radial edges by a combination of the Rayleigh-Ritz method and coordinate transformation. Swaminadham *et al*. (1984) compared the natural frequencies of annular sector plates from the finite element method and experiments. Seok and

*Corresponding author, Ph.D.,
E-mail: vahid.th1982@gmail.com;
vahid.tahouneh@ut.ac.ir

ISSN: 1229-9367 (Print), 1598-6233 (Online)

Tiersten (2004) used a variational approximation procedure to analyze the free vibration of cantilevered annular sector plates. Houmat (2001) used the hierarchical finite element method to study the free vibration of annular sector plates. Marin (2008) used some general results from the general theory of elliptic equations in order to obtain some qualitative results in a concrete and very applicative situation. In fact, he proved the existence and uniqueness of the generalized solutions for the boundary value problems in elasticity of initially stressed bodies with voids (porous materials). Marin *et al*. (2013) considered a theory of thermoelasticity constructed by taking into account the heat conduction in deformable bodies which depends on two temperatures. Marin (2016) investigated a micropolar porous body, including voidage time derivative among the independent constitutive variables. Marin and Baleanu (2016) studied vibrations in thermoelasticity without energy dissipation for micropolar bodies. With the help of a measure associated with the corresponding steady-state vibration and by assuming that the exciting frequency is lower than a certain critical frequency, they obtained a spatial decay estimate. Sharma *et al*. (2005a, b) integrated an analytical approach with the Chebyshev polynomials technique to study the buckling and free vibration of isotropic and laminated composite sector plates based on the first-order shear deformation theory. For moderate thickness plates, the first-order shear deformable plate theory is commonly used, which could provide a result more accurate than that from the CPT. Liew and Liu (2000) used the differential quadrature method to analyze the free vibration of thick annular sector plates. Barka *et al*. (2016) studied Thermal post-buckling behavior of imperfect temperature-dependent sandwich FG plates. Bouguenina *et al*. (2015) studied FG plates with variable thickness subjected to thermal buckling. Chen *et al*. (2017) studied Vibration and stability of initially stressed sandwich plates with FGM face sheets. Wu and Liu (2016) developed a state space differential reproducing kernel (DRK) method in order to study 3D analysis of FG circular plates. Park *et al*. (2016) used modified couple stress for dynamic analysis of sigmoid functionally graded materials plates. Leissa *et al*. (1993) and McGee *et al*. (1995) considered the effect of stress singularities on the vibration analysis of thick annular sector plates and presented the corner functions to improve the convergence of the numerical solutions. Zhou *et al*. (2009) used the Chebyshev-Ritz method to study the free vibration of thick annular sector plates, Nie and Zhong (2008) investigated the free and forced vibration analysis of FGM annular sector plates with simply-supported radial edges by using a semi-analytical approach. Arefi (2015) suggested an analytical solution of a curved beam with different shapes made of functionally graded materials (FGMs). Bennai *et al*. (2015) developed a new refined hyperbolic shear and normal deformation beam theory to study the free vibration and buckling of functionally graded (FG) sandwich beams under various boundary conditions. Bouchafa *et al*. (2015) used refined hyperbolic shear deformation theory (RHSDT) for the thermoelastic bending analysis of functionally graded sandwich plates. Tahouneh (2016) presented a 3-D elasticity solution for free vibration analysis of continuously graded carbon nanotube-reinforced (CGCNTR) rectangular plates resting on two-parameter elastic foundations. The volume fractions of oriented, straight single-walled carbon nanotubes (SWCNTs) were assumed to be graded in the thickness direction. Moradi-Dastjerdi and Momeni-Khabisi (2016) studied Free and forced vibration of plates reinforced by wavy carbon nanotube (CNT). The plates were resting on Winkler-Pasternak elastic foundation and subjected to periodic or impact loading. Kamarian *et al*. (2015) studied vibration analysis of sandwich beams. The material properties of the FG nanocomposite sandwich beam are estimated using the Eshelby-Mori-Tanaka approach. Tornabene *et al*. (2016) investigated the effect of Carbon Nanotube (CNT) agglomeration on the free vibrations of laminated composite doubly-curved shells and panels reinforced by CNTs. Fantuzzi *et al*. (2017) studied free vibration of arbitrarily shaped FG carbon nanotube-reinforced plates using generalized differential quadrature method. Some additional parametric studies were also performed to analyze the effect of a mesh distortion, by considering several geometric and mechanical configurations. Tornabene *et al*. (2017a) investigated the static response of composite plates and shells reinforced by agglomerated nanoparticles made of carbon nanotubes. A two-parameter agglomeration model was taken into account to describe the micromechanics of such particles, which showed the tendency to agglomerate into spherical regions when scattered in a polymer matrix. A survey of several methods under the heading of strong formulation finite element method (SFEM) was presented by Tornabene *et al*. (2015). These approaches were distinguished from classical one, termed weak formulation finite element method (WFEM). Free vibration analysis of Carbon Nanotube-Reinforced Composite (CNTRC) conical shells was performed considering the agglomeration effect of Carbon Nanotubes (CNTs) by Kamarian *et al*. (2016). Tornabene *et al*. (2017b) investigated free vibration problem of sandwich shell structures with variable thickness and made of Functionally Graded Materials (FGMs). Several Higher-order Shear Deformation Theories (HSDTs), defined by a unified formulation, were employed in their study. A comparative study between different analytical and numerical three-dimensional (3D) and two-dimensional (2D) shell models for the bending analysis of composite and sandwich plates, spherical and doubly-curved shells subjected to a transverse normal load applied at the top surface was presented by Tornabene and Brischetto (2018). A study for comparison between different shell models in the case of static analysis of multilayered composite and sandwich plates and spherical shells was carried out by Tornabene and Brischetto (2018). Transverse shear loads were applied on these structures. The behavior through the thickness direction was analyzed in terms of the three displacement components and the six stress components. Based on the three-dimensional elasticity theory, free vibration analysis of sandwich plate and panel were carried out using GDQ method (Kamarian *et al*. 2013, 2014). The two-constituent functionally graded shell consisted of ceramic and metal. These constituents were graded through

the thickness according to a generalized power-law distribution.

Nowadays, the use of carbon nanotubes in polymer/carbon nanotube composites has attracted wide attention (Wagner *et al*. 1997). A high aspect ratio, low weight of CNTs and their extraordinary mechanical properties (strength and flexibility) provide the ultimate reinforcement for the next generation of extremely lightweight but highly elastic and very strong advanced composite materials. On the other hand, by using of the polymer/CNT composites in advanced composite materials, we can achieve structures with low weight, high strength and high stiffness in many structures of civil, mechanical and space engineering.

Several researches have recently investigated the elastic properties of multiwalled carbon nanotube (MWCNT) and their composites (Fidelus *et al*. 2005, Ghavamian *et al*. 2012). Farsadi *et al*. (2013) investigated the extent to which the effective stiffness of composite materials can be impacted by the characteristic waviness of nanotubes embedded in polymers. Weidt and Figiel (2015) developed a 3D nonlinear computational model to predict the compressive behaviour of epoxy/carbon nanotube (CNT). Gojny *et al*. (2005) focused on the evaluation of the different types of the CNTs applied, their influence on the mechanical properties of epoxy-based nanocomposites and the relevance of surface functionalization. Therefore, the study of the mechanical performance of CNT-based composites and the discovery of possible innovative applications has recently attracted the interest of many researchers. Several researchers have reported that mechanical properties of polymeric matrices can be drastically increased (Montazeri *et al*. 2010, Yeh *et al*. 2006) by adding a few weight percent (wt%) MWCNTs. Montazeri *et al*. (2010) showed that modified Halpin-Tsai equation with exponential Aspect ratio can be used to model the experimental result of MWNT composite samples. They also demonstrated that reduction in Aspect ratio (L/d) and nanotube length cause a decrease in aggregation and Above 1.5wt%, nanotubes agglomerate causing a reduction in Young's modulus values. Thus, it is important to determine the effect Aspect ratio and arrangement of CNTs on the effective properties of carbon nanotube-reinforced composite (CNTRC). The stiffening effect of carbon nanotubes was quantitatively investigated by micro-mechanics methods. Especially, the effects of the extensively observed waviness and agglomeration of carbon nanotubes were examined theoretically by Shi *et al*. (2004). Yeh *et al*. (2006) used the Halpin-Tsai equation to shows the effect of MWNT shape factor (L/d) on the mechanical properties. They showed that the mechanical properties of nanocomposite samples with the higher shape factor (L/d) values were better than the ones with the lower shape factor. The reinforcement effect of MWCNTs with different aspect ratio in an epoxy matrix has been carried out by Martone *et al*. (2011). They showed that progressive reduction of the tubes effective aspect ratio occurs because of the increasing connectedness between tubes upon an increase in their concentration. Also they investigated on the effect of nanotube curvature on the average contacts number between tubes by means of the waviness that accounts for the deviation from the straight particles assumption. The material properties of FG-CNTR can be evaluated through a micromechanical model in which CNT efficiency parameters are estimated by matching the elastic moduli of the CNTR observed from the molecular dynamics (MD) simulation with that of numerical results obtained from the rule of mixture (Shen 2009).

Analysis of FG-CNTR plates were first presented by Shen (2009) in which he studied the nonlinear bending behavior of FG-CNTR plates in thermal environment. He concluded that the load bending moment curves of the plate could be significantly increased as a result of functionally graded CNT reinforcements. Shen and Zhang (2010) presented thermal buckling and post buckling behavior of functionally graded nanocomposite plates reinforced by single-walled carbon nanotubes (SWCNTs). The temperature-dependent material properties of SWCNTs were obtained from MD simulations. In comparison with research works on the free vibration or buckling analyses of FG structures, only a few references can be found that consider the effect of waviness and aspect ratio on the free vibrational behavior of panels with four edges simply supported (Moradi-Dastjerdi *et al*. 2013). Moradi-Dastjerdi *et al*. (2013) investigated the effects of CNT waviness on the dynamic behavior of FG-CNTR cylinder under impact load. Tornabene *et al*. (2018) studied free vibration of laminated nano-composite plates and shells using first-order shear deformation theory and the Generalized Differential Quadrature (GDQ) method. Each layer of the laminate was modelled as a three-phase composite. Despite the aforementioned extensive research on the free vibration analysis of structures resting on elastic foundations, to the authors' best knowledge, still very little work has been done for vibration analysis of FG-CNTR structures and considering the effect of waviness and aspect ratio on their vibrational response. The aim of this study is to fill this apparent gap in this area by investigating the effects of CNTs waviness and aspect ratio on vibrational behavior of FG sandwich annular sector plates on elastic foundations. Five linear types of distributions of CNTs are considered; uniform and four kinds of FG distributions along the thickness of face sheets and the effects of CNT volume fraction, aspect ratio and waviness and also Pasternak's elastic foundation coefficients, sandwich plate thickness, face sheets thickness and plate aspect ratio are investigated on the free vibration behavior of sandwich plates with wavy CNT-reinforced face sheets.

2. Problem description

2.1 Mechanical properties of the sandwich structure

Consider a sandwich annular sector plate resting on two-parameter elastic foundations as shown in Fig. 1. This plate is referring to a cylindrical coordinate system (r, θ, z), as depicted in Fig. 1. It is assumed that the total thickness of plate is "h". Volume fraction of CNT is assumed to be graded along the thickness of the face sheets. The FG-

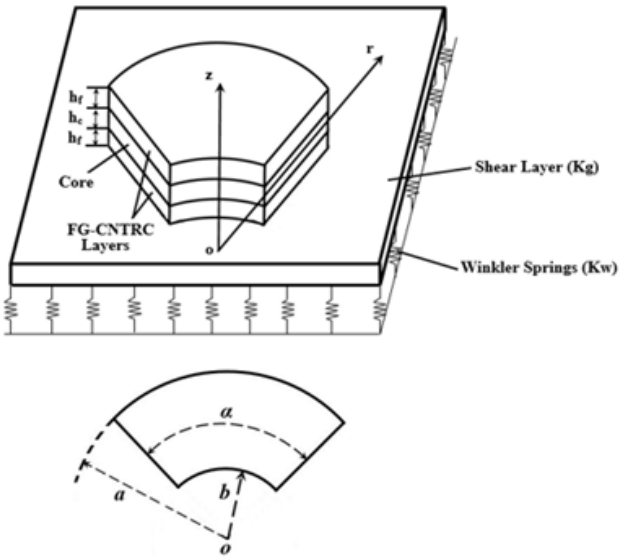

Fig. 1 Geometry of the sandwich annular sector plate on an elastic foundation

CNTRC face sheets are made from a mixture of wavy SWCNTs and isotropic matrix.

The wavy SWCNT reinforcement is either uniformly distributed (UD) or functionally graded in the plate thickness.

Employing the extended rule of mixture the effective elastic properties of the CNTR plate can be expressed as follows (Shen 2009)

$$E_{11} = \eta_1 V_{CNT} E^{CNT}_{11,\eta^*} + V_m E^m \tag{1}$$

$$\frac{\eta_2}{E_{22}} = \frac{V_{CNT}}{E^{CNT}_{22,\eta^*}} + \frac{V_m}{E^m} \tag{2}$$

$$\frac{\eta_3}{G_{12}} = \frac{V_{CNT}}{G^{CNT}_{12,\eta^*}} + \frac{V_m}{G^m} \tag{3}$$

$$\upsilon_{12} = V_{CNT}\,\upsilon^{CNT}_{12} + V_m \upsilon^m \tag{4}$$

$$\rho = V_{CNT}\,\rho^{CNT} + V_m \rho^m \tag{5}$$

where $E^{CNT}_{\eta^*}$, E^{CNT}_{22,η^*}, G^{CNT}_{12,η^*}, υ^{CNT}_{12} and ρ^{CNT} denote effective Young's moduli, effective shear modulus, Poisson's ratios and density of the CNT, respectively. E^m, G^m, υ^m and ρ^m are the corresponding properties of the isotropic matrix. η_j (j = 1, 2, 3) are the CNT efficiency parameters accounting for the scale-dependent material properties evaluated by comparing the effective material properties obtained from MD simulations and that of numerical results obtained from the rule of mixture in (Shen 2009). V_{CNT} and V_m are the CNT and matrix volume fractions related by

$$V_{CNT} + V_m = 1 \tag{6}$$

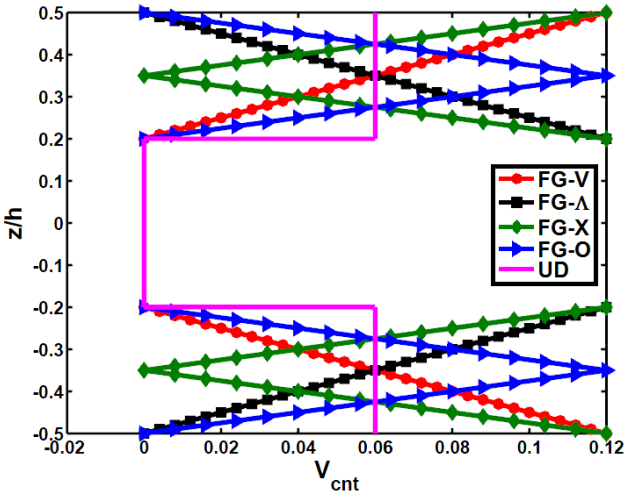

Fig. 2 Variation of nanotube volume fraction (V_{cnt}) along the thickness of plate for different CNT distributions

The effective Young's moduli and shear modulus of wavy CNT are introduced as follows (Martone *et al*. 2011)

$$E^{CNT}_{ii,\eta^*} = \eta^* E^{CNT}_{ii}, i = 1,2$$
$$G^{CNT}_{12,\eta^*} = \eta^* G^{CNT}_{12} \tag{7}$$

where

$$\eta^* = 1 - \frac{tanh(K.AR/(1+<c>))}{K.AR/(1+<c>)}$$
$$K = \sqrt{\frac{-2}{1+\upsilon_m} / \left(\frac{E^{CNT}_{11}}{E^m_{11}} ln V_{CNT}\right)} \tag{8}$$

The efficiency parameter, η^*, is considered to account the CNT aspect ratio and waviness (Martone *et al*. 2011). <*c*> is the average number of contacts for CNTs depends on their aspect ratio defined as

$$<c> = wV_{CNT} + \left(4 + \frac{3AR^2}{3AR+2}\right) \tag{9}$$

where the waviness, *w*, has been introduced for accounting the CNT's curvature within the CNTR structure (Martone *et al*. 2011). Introducing this parameter, the excluded volume due to the curvature of CNTs has been considered. The accuracy of this method has been investigated by Moradi-Dastjerdi *et al*. (2013). The variation of CNT distribution through the plate thickness is assumed as follows (Fig. 2)

$$FG-V: \begin{Bmatrix} V_{CNT} = 2\left(1 + \frac{z - h/2}{h_f}\right) V^*_{CNT}, for \quad 0.2 < z/h < 0.5 \\ V_{CNT} = 2\left(1 + \frac{-z - h/2}{h_f}\right) V^*_{CNT}, for \quad -0.5 < z/h < -0.2 \end{Bmatrix},$$
$$FG-\Lambda: \begin{Bmatrix} V_{CNT} = -2\left(\frac{2z - h}{2h_f}\right) V^*_{CNT}, for \quad 0.2 < z/h < 0.5 \\ V_{CNT} = 2\left(\frac{2z + h}{2h_f}\right) V^*_{CNT}, for \quad -0.5 < z/h < -0.2 \end{Bmatrix}, \tag{10}$$

$$FG-X:\begin{Bmatrix} V_{CNT}=2(1+\frac{2}{h_f}(z-h/2))V_{CNT}^{*}, for\ \ 0.35<z/h<0.5 \\ V_{CNT}=2(-1-\frac{2}{h_f}(z-h/2))V_{CNT}^{*}, for\ \ 0.2<z/h<0.35 \\ V_{CNT}=2(-1-\frac{2}{h_f}(-z-h/2))V_{CNT}^{*}, for\ \ -0.35<z/h<-0.2 \\ V_{CNT}=2(1+\frac{2}{h_f}(-z-h/2))V_{CNT}^{*}, for\ \ -0.5<z/h<-0.35 \end{Bmatrix},$$

$$FG-\Diamond:\begin{Bmatrix} V_{CNT}=\frac{4}{h_f}(-z+h/2)V_{CNT}^{*}, for\ \ 0.35<z/h<0.5 \\ V_{CNT}=\frac{4}{h_f}(z-h/2+h_f)V_{CNT}^{*}, for\ \ 0.2<z/h<0.35 \\ V_{CNT}=\frac{4}{h_f}(-z-h/2+h_f)V_{CNT}^{*}, for\ \ -0.35<z/h<-0.2 \\ V_{CNT}=\frac{4}{h_f}(z+h/2)V_{CNT}^{*}, for\ \ -0.5<z/h<-0.35 \end{Bmatrix}, \quad (10)$$

$$UD:\begin{Bmatrix} V_{CNT}=V_{CNT}^{*}, for\ \ 0.2<z/h<0.5 \\ V_{CNT}=V_{CNT}^{*}, for\ \ -0.5<z/h<-0.2 \end{Bmatrix}$$

where

$$V_{CNT}^{*}=\frac{w_{CNT}}{w_{CNT}+(\rho^{CNT}/\rho^{m})(1-w_{CNT})} \quad (11)$$

V_{CNT}^{*} is the CNT volume fraction and w_{CNT} is the mass fraction of CNTs. Poly methyl methacrylate, referred to as PMMA and (10,10) SWCNTs are selected as the matrix and the reinforcement materials, respectively. The material properties for the constituent materials are listed in Table 1 (Shen and Zhang 2010).

Values of CNT efficiency parameters, η_i (i = 1, 2, 3), for different CNT volume fractions are presented in Table 2 to capture the scale difference between micro and nano levels. It should be noted that $\eta_3 = 0.7\eta_2$, $G_{13} = G_{12}$ and $G_{23} = 1.2G_{12}$ (Shen and Zhang 2010).

Table 1 Properties of the (10,10) SWCNT and the polymer matrix (Shen and Zhang 2010)

SWCNT	Polymer matrix
E_{11}^{CNT} = 5.6466 (TPa),	
E_{22}^{CNT} = 7.0800 (TPa),	E^m = 2.1 (GPa)
G_{12}^{CNT} =1.9447 (TPa),	ρ^m = 1150 (kg/m^3)
ρ^{CNT} = 1400 (kg/m^3)	υ^m = 034
υ_{12} = 0.175	

Table 2 CNT efficiency parameters for different values of volume fractions (Shen and Zhang 2010)

V_{CNT}^{*}	η_1	η_2	η_3
0.12	0.137	1.022	0.715
0.17	0.142	1.626	1.138
0.28	0.141	1.585	1.109

3. Governing equations

In the absence of body forces, the governing equations are as follows (Reddy 2013)

$$\begin{aligned} &\frac{\partial\sigma_r}{\partial r}+\frac{1}{r}\frac{\partial\tau_{r\theta}}{\partial\theta}+\frac{\partial\tau_{rz}}{\partial z}+\frac{\sigma_r-\sigma_\theta}{r}=\rho\frac{\partial^2 u_r}{\partial t^2} \\ &\frac{\partial\tau_{r\theta}}{\partial r}+\frac{1}{r}\frac{\partial\sigma_\theta}{\partial\theta}+\frac{\partial\tau_{\theta z}}{\partial z}+\frac{2\tau_{r\theta}}{r}=\rho\frac{\partial^2 u_\theta}{\partial t^2} \\ &\frac{\partial\tau_{rz}}{\partial r}+\frac{1}{r}\frac{\partial\tau_{\theta z}}{\partial\theta}+\frac{\partial\sigma_z}{\partial z}+\frac{\tau_{rz}}{r}=\rho\frac{\partial^2 u_z}{\partial t^2} \end{aligned} \quad (12)$$

where σ_r, σ_θ, σ_z are axial stress components, $\tau_{r\theta}$, $\tau_{\theta z}$, τ_{rz} are shear stress components, u_r, u_θ, u_z are displacement components, ρ denotes material density and t is time. The relations between the strain and the displacement are

$$\begin{aligned} &\varepsilon_r=\frac{\partial u_r}{\partial r},\varepsilon_\theta=\frac{u_r}{r}+\frac{1}{r}\frac{\partial u_\theta}{\partial\theta},\varepsilon_z=\frac{\partial u_z}{\partial z}, \\ &\gamma_{\theta z}=\frac{\partial u_\theta}{\partial z}+\frac{1}{r}\frac{\partial u_z}{\partial\theta},\gamma_{rz}=\frac{\partial u_r}{\partial z}+\frac{\partial u_z}{\partial r}, \\ &\gamma_{r\theta}=\frac{1}{r}\frac{\partial u_r}{\partial\theta}+\frac{\partial u_\theta}{\partial r}-\frac{u_\theta}{r} \end{aligned} \quad (13)$$

where ε_r, ε_θ, ε_z, $\gamma_{\theta z}$, $\gamma_{r\theta}$, γ_{rz} are strain components. The constitutive equations for material are (Reddy 2013)

$$\begin{Bmatrix}\sigma_r\\ \sigma_\theta\\ \sigma_z\\ \tau_{z\theta}\\ \tau_{rz}\\ \tau_{r\theta}\end{Bmatrix}=\begin{bmatrix} c_{11} & c_{12} & c_{13} & 0 & 0 & 0 \\ c_{12} & c_{22} & c_{23} & 0 & 0 & 0 \\ c_{13} & c_{23} & c_{33} & 0 & 0 & 0 \\ 0 & 0 & 0 & c_{44} & 0 & 0 \\ 0 & 0 & 0 & 0 & c_{55} & 0 \\ 0 & 0 & 0 & 0 & 0 & c_{66} \end{bmatrix}\begin{Bmatrix}\varepsilon_r\\ \varepsilon_\theta\\ \varepsilon_z\\ \gamma_{z\theta}\\ \gamma_{rz}\\ \gamma_{r\theta}\end{Bmatrix} \quad (14)$$

where c_{ij} are material elastic stiffness coefficients.

Using the three-dimensional constitutive relations and the strain-displacement relations, the equations of motion in terms of displacement components for a linear elastic FG plate with infinitesimal deformations can be written as

$$\begin{aligned} &c_{11}\frac{\partial^2 u_r}{\partial r^2}+c_{12}\left(-\frac{1}{r^2}\frac{\partial u_\theta}{\partial\theta}+\frac{1}{r}\frac{\partial^2 u_\theta}{\partial r\partial\theta}+\frac{1}{r}\frac{\partial u_r}{\partial r}-\frac{1}{r^2}u_r\right) \\ &+c_{13}\frac{\partial^2 u_z}{\partial r\partial z}+\frac{c_{66}}{r}\left(\frac{\partial^2 u_\theta}{\partial\theta\partial r}+\frac{1}{r}\frac{\partial^2 u_r}{\partial\theta^2}-\frac{1}{r}\frac{\partial u_\theta}{\partial\theta}\right) \\ &c'_{55}\left(\frac{\partial u_r}{\partial z}+\frac{\partial u_z}{\partial r}\right)+c_{55}\left(\frac{\partial^2 u_r}{\partial z^2}+\frac{\partial^2 u_z}{\partial z\partial r}\right)+ \\ &\frac{1}{r}\left[c_{11}\frac{\partial u_r}{\partial r}+c_{12}\left(\frac{1}{r}\frac{\partial u_\theta}{\partial\theta}+\frac{u_r}{r}\right)+c_{13}\frac{\partial u_z}{\partial z}-c_{12}\frac{\partial u_r}{\partial r}\cdot\right. \\ &\left.-c_{22}\left(\frac{1}{r}\frac{\partial u_\theta}{\partial\theta}+\frac{u_r}{r}\right)-c_{23}\frac{\partial u_z}{\partial z}\right]=\rho\frac{\partial^2 u_r}{\partial t^2} \end{aligned} \quad (15)$$

$$
\begin{aligned}
&c_{66}\left(\frac{\partial^2 u_\theta}{\partial r^2}-\frac{1}{r^2}\frac{\partial u_r}{\partial \theta}+\frac{1}{r}\frac{\partial^2 u_r}{\partial r\partial \theta}+\frac{1}{r^2}u_\theta-\frac{1}{r}\frac{\partial u_\theta}{\partial r}\right)\\
&+\frac{1}{r}\left[c_{12}\frac{\partial^2 u_r}{\partial \theta \partial r}+c_{22}\left(\frac{1}{r}\frac{\partial^2 u_\theta}{\partial \theta^2}+\frac{1}{r}\frac{\partial u_r}{\partial \theta}\right)+c_{23}\frac{\partial^2 u_z}{\partial \theta \partial z}\right]\\
&+c'_{44}\left(\frac{1}{r}\frac{\partial u_z}{\partial \theta}+\frac{\partial u_\theta}{\partial z}\right)+c_{44}\left(\frac{1}{r}\frac{\partial^2 u_z}{\partial z\partial \theta}+\frac{\partial^2 u_\theta}{\partial z^2}\right)\\
&+\frac{2c_{66}}{r}\left(\frac{\partial u_\theta}{\partial r}+\frac{1}{r}\frac{\partial u_r}{\partial \theta}-\frac{u_\theta}{r}\right)=\rho\frac{\partial^2 u_\theta}{\partial t^2}
\end{aligned}
\tag{16}
$$

$$
\begin{aligned}
&c_{55}\left(\frac{\partial^2 u_r}{\partial r\partial z}+\frac{\partial^2 u_z}{\partial r^2}\right)+\frac{c_{44}}{r}\left(\frac{1}{r}\frac{\partial^2 u_z}{\partial \theta^2}+\frac{\partial^2 u_\theta}{\partial \theta \partial z}\right)\\
&+c'_{13}\frac{\partial u_r}{\partial r}+c_{13}\frac{\partial^2 u_r}{\partial z\partial r}+c'_{23}\left(\frac{1}{r}\frac{\partial u_\theta}{\partial \theta}+\frac{u_r}{r}\right)\\
&+c_{23}\left(\frac{1}{r}\frac{\partial^2 u_\theta}{\partial z\partial \theta}+\frac{1}{r}\frac{\partial u_r}{\partial z}\right)+c'_{33}\frac{\partial u_z}{\partial z}+c_{33}\frac{\partial^2 u_z}{\partial z^2}\\
&+\frac{c_{55}}{r}\left(\frac{\partial u_r}{\partial z}+\frac{\partial u_z}{\partial r}\right)=\rho\frac{\partial^2 u_z}{\partial t^2}
\end{aligned}
\tag{17}
$$

where $c'_{ij}=\frac{dc_{ij}}{dz}$.

Eqs. (15) and (16) represent the in-plane equations of motion along the r and θ-axes, respectively; and Eq. (17) is the transverse or out-of-plane equation of motion.

The related boundary conditions are as follows:

at $z = -0.5h$

$$
\begin{aligned}
&\tau_{zr}=0,\tau_{z\theta}=0\\
&\sigma_z=K_w u_z-K_g\left(\frac{\partial^2 u_z}{\partial r^2}+\frac{1}{r}\frac{\partial u_z}{\partial r}+\frac{1}{r^2}\frac{\partial^2 u_z}{\partial \theta^2}\right)
\end{aligned}
\tag{18}
$$

at $z = 0.5h$

$$
\tau_{zr}=0,\tau_{z\theta}=0,\sigma_z=0 \tag{19}
$$

K_w and K_g are the Winkler and shearing layer elastic coefficients of the foundation. In this paper three different kinds of boundary conditions are considered for circular edges including clamped-clamped (c-c), simply supported-clamped (s-c) and free-clamped (f-c). The boundary conditions at edges are

Clamped ($r = b$)-Clamped ($r = a$)

$$
\begin{aligned}
&\text{at}\quad r=a \qquad u_r=u_\theta=u_z=0\\
&\text{at}\quad r=b \qquad u_r=u_\theta=u_z=0
\end{aligned}
\tag{20}
$$

Simply supported ($r = b$)-Clamped ($r = a$)

$$
\begin{aligned}
&\text{at}\quad r=b \qquad u_\theta=u_z=\sigma_r=0\\
&\text{at}\quad r=a \qquad u_r=u_\theta=u_z=0
\end{aligned}
\tag{21}
$$

Free ($r = b$)-Clamped ($r = a$)

$$
\begin{aligned}
&\text{at}\quad r=a \qquad u_r=u_\theta=u_z=0\\
&\text{at}\quad r=b \qquad \sigma_r=\tau_{r\theta}=\tau_{rz}=0
\end{aligned}
\tag{22}
$$

4. Solution procedure

Using the geometrical periodicity of the plate, the displacement components for the free vibration analysis canbe represented as

$$
\begin{aligned}
&U_r(r,\theta,z,t)=U_{rm}(r,z)\sin(m\pi\theta/\alpha)e^{i\omega t},\\
&U_\theta(r,\theta,z,t)=U_{\theta m}(r,z)\cos(m\pi\theta/\alpha)e^{i\omega t},\\
&U_z(r,\theta,z,t)=U_{zm}(r,z)\sin(m\pi\theta/\alpha)e^{i\omega t}
\end{aligned}
\tag{23}
$$

where m (= 0, 1,…, ∞) is the circumferential wavenumber; ω is the natural frequency and i $(=\sqrt{-1})$ is the imaginary number. It is obvious that m = 0 means axisymmetric vibration. At this stage the generalized differential quadrature (GDQ) method [A brief review of GDQ method is given in Appendix] rules are employed to discretize the free vibration equations and the related boundary conditions. Substituting for the displacement components from (23) and then using the GDQ rules for the spatial derivatives, the discretized form of the equations of motion at each domain grid point (r_j, z_k) with (j = 2, 3,…, N_r – 1) and (k = 2, 3,…, N_z – 1) can be obtained as

Eq. (15)

$$
\begin{aligned}
&(c_{11})_k\sum_{n=1}^{N_r}B^r_{jn}u_{rmnk}+(c_{12})_k\left(\frac{m\pi}{r_j^2\alpha}u_{\theta mjk}-\frac{m\pi}{r_j\alpha}\right.\\
&\left.\sum_{n=1}^{N_r}A^r_{jn}u_{\theta mnk}+\frac{1}{r_j}\sum_{n=1}^{N_r}A^r_{jn}u_{rmnk}-\frac{1}{r_j^2}u_{rmjk}\right)\\
&+(c_{13})_k\sum_{n=1}^{N_r}\sum_{r=1}^{N_z}A^r_{jn}A^z_{kr}u_{zmnr}+\frac{(c_{66})_k}{r_j}\left(-\frac{m\pi}{\alpha}\sum_{n=1}^{N_r}A^r_{jn}u_{\theta mnk}\right.\\
&\left.-\frac{m^2\pi^2}{r_j\alpha^2}u_{rmjk}+\frac{m\pi}{r_j\alpha}u_{\theta mjk}\right)+(c'_{55})_k\\
&\left(\sum_{n=1}^{N_z}A^z_{kn}u_{rmjn}+\sum_{n=1}^{N_r}A^r_{jn}u_{zmnk}\right)\\
&+(c_{55})_k\left(\sum_{n=1}^{N_z}B^z_{kn}u_{rmjn}+\sum_{n=1}^{N_r}\sum_{r=1}^{N_z}A^r_{jn}A^z_{kr}u_{zmnr}\right)\\
&+\frac{1}{r_j}\left((c_{11})_k\sum_{n=1}^{N_r}A^r_{jn}u_{rmnk}+(c_{12})_k\left(\frac{m\pi}{r_j\alpha}u_{\theta mjk}+\frac{1}{r_j}u_{rmjk}\right)\right.\\
&+(c_{13})_k\sum_{n=1}^{N_z}A_{kn}u_{zmjn}-(c_{12})_k\sum_{n=1}^{N_r}A^r_{jn}u_{rmnk}\\
&-(c_{22})_k\left(-\frac{m\pi}{r_j\alpha}u_{\theta mjk}+\frac{1}{r_j}u_{rmjk}\right)-(c_{23})_k\sum_{n=1}^{N_z}A^z_{kn}u_{zmjn})\\
&=-\rho_k\omega^2u_{rmjk}
\end{aligned}
\tag{24}
$$

Eq. (16)

$$
(c_{66})_k\left(\sum_{n=1}^{N_r}B^r_{jn}u_{\theta mnk}-\frac{m\pi}{r_j^2\alpha}u_{rmjk}+\frac{m\pi}{r_j\alpha}\sum_{n=1}^{N_r}A^r_{jn}u_{rmnk}+\right. \tag{25}
$$

$$\begin{aligned}
&\frac{1}{r_j^2}u_{\theta mjk}-\frac{1}{r_j}\sum_{n=1}^{N_r}A_{jn}^{r}u_{\theta mnk})+\frac{1}{r_j}((c_{12})_k(\frac{m\pi}{\alpha})\sum_{n=1}^{N_r}A_{jn}^{r}u_{rmnk}\\
&+(c_{22})_k\left(-\frac{m^2\pi^2}{r_j\alpha^2}u_{\theta mjk}+\frac{m\pi}{r_j\alpha}u_{rmjk}\right)+(c_{23})_k(\frac{m\pi}{\alpha})\sum_{n=1}^{N_z}A_{kn}^{z}u_{zmjn}\\
&+(c'_{44})_k\left(\frac{m\pi}{r_j\alpha}u_{zmjk}+\sum_{n=1}^{N_z}A_{kn}^{z}u_{\theta mjn}\right)\\
&+(c_{44})_k(\frac{m\pi}{r_j\alpha}\sum_{n=1}^{N_z}A_{kn}^{z}u_{zmjn}+\sum_{n=1}^{N_z}B_{kn}^{z}u_{\theta mjn})+\frac{2(c_{66})_k}{r_j}\\
&(\sum_{n=1}^{N_r}A_{jn}^{r}u_{\theta mnk}+\frac{m\pi}{r_j\alpha}u_{rmjk}-\frac{u_{\theta mjk}}{r_j})\\
&=-\rho_k\omega^2u_{\theta mjk}
\end{aligned}\tag{25}$$

Eq. (17)

$$\begin{aligned}
&(c_{55})_k\left(\sum_{n=1}^{N_r}\sum_{r=1}^{N_z}A_{kr}^{z}A_{jn}^{r}u_{rmnr}+\sum_{n=1}^{N_r}B_{jn}^{r}u_{zmnk}\right)\\
&+\frac{(c_{44})_k}{r_j}(\frac{-m^2\pi^2}{r_j\alpha^2}u_{zmjk}-\frac{m\pi}{\alpha}\sum_{n=1}^{N_z}A_{kn}^{z}u_{\theta mjn})\\
&+(c'_{13})_k\sum_{n=1}^{N_z}A_{kn}^{z}u_{rmjn}+(c_{13})_k\sum_{n=1}^{N_r}\sum_{r=1}^{N_z}A_{kr}^{z}A_{jn}^{r}u_{rmnr}\\
&+(c'_{23})_k(-\frac{m\pi}{r_j\alpha}u_{\theta mjk}+\frac{u_{rmjk}}{r_j})+(c_{23})_k\\
&(-\frac{m\pi}{r_j\alpha}\sum_{n=1}^{N_z}A_{kn}^{z}u_{\theta mjn}+\frac{1}{r_j}\sum_{n=1}^{N_z}A_{kn}^{z}u_{rmjn})+(c'_{33})_k\sum_{n=1}^{N_z}A_{kn}^{z}u_{zmjn}\\
&+(c_{33})_k\sum_{n=1}^{N_z}B_{kn}^{z}u_{zmjn}+\frac{(c_{55})_k}{r_j}(\sum_{n=1}^{N_z}A_{kn}^{z}u_{rmjn}\\
&+\sum_{r=1}^{N_r}A_{jr}^{r}u_{zmrk})=-\rho_k\omega^2u_{zmjk}
\end{aligned}\tag{26}$$

where A_{ij}^{r}, A_{ij}^{z} and B_{ij}^{r}, B_{ij}^{z} are the first and second order GDQ weighting coefficients in the *r*- and *z*- directions, respectively.

In a similar manner the boundary conditions can be discretized. For this purpose, using Eq. (23) and the GDQ discretization rules for spatial derivatives, the boundary conditions at $z = 0$ and h become,

Eq. (18)

at $z = -0.5$h

$$\begin{aligned}
&\sum_{n=1}^{N_z}A_{kn}^{z}u_{rmjn}+\sum_{n=1}^{N_r}A_{jn}^{r}u_{zmnk}=0,\\
&\frac{m\pi}{r_j\alpha}u_{zmjk}+\sum_{n=1}^{N_z}A_{kn}^{z}u_{\theta mjn}=0,\\
&(c_{13})_k(\sum_{n=1}^{N_r}A_{jn}^{r}u_{rmnk})+(c_{23})_k(-\frac{m\pi}{r_j\alpha}u_{\theta mjk}+\frac{1}{r_j}u_{rmjk})\\
&+(c_{33})_k(\sum_{n=1}^{N_z}A_{kn}^{z}u_{zmjn})-K_wu_{zmjk}+K_g\\
&(\sum_{n=1}^{N_r}B_{jn}^{r}u_{zmnk}+\frac{1}{r_j}\sum_{n=1}^{N_r}A_{jn}^{r}u_{zmnk}-\frac{m^2\pi^2}{r_j^2\alpha^2}u_{zmjk})=0
\end{aligned}\tag{27}$$

Eq. (19)

at $z = 0.5$h

$$\begin{aligned}
&\sum_{n=1}^{N_z}A_{kn}^{z}u_{rmjn}+\sum_{n=1}^{N_r}A_{jn}^{r}u_{zmnk}=0,\\
&\frac{m\pi}{r_j\alpha}u_{zmjk}+\sum_{n=1}^{N_z}A_{kn}^{z}u_{\theta mjn}=0,\\
&(c_{13})_k(\sum_{n=1}^{N_r}A_{jn}^{r}u_{rmnk})+(c_{23})_k(-\frac{m\pi}{r_j\alpha}u_{\theta mjk}+\frac{1}{r_j}u_{rmjk})\\
&+(c_{33})_k(\sum_{n=1}^{N_z}A_{kn}^{z}u_{zmjn})=0
\end{aligned}\tag{28}$$

where $k = 1$ at $z = -0.5$h and $k = N_z$ at $z = 0.5$h, and $j = 1, 2, \ldots, N_r$. The boundary conditions at $r = b$ and a stated in (20-22) become,

Simply supported (S)

$$\begin{aligned}
&u_{zmjk}=0,u_{\theta mjk}=0,\\
&(c_{11})_k(\sum_{n=1}^{N_r}A_{jn}^{r}u_{rmnk})+(c_{12})_k(-\frac{m\pi}{r_j\alpha}u_{\theta mjk}+\frac{1}{r_j}u_{rmjk})\\
&+(c_{13})_k(\sum_{n=1}^{N_z}A_{kn}^{z}u_{zmjn})=0
\end{aligned}\tag{29a}$$

Clamped (C)

$$u_{rmjk}=0,u_{\theta mjk}=0,u_{zmjk}=0\tag{29b}$$

Free (F)

$$\begin{aligned}
&(c_{11})_k\sum_{n=1}^{N_r}A_{jn}^{r}u_{rmnk}+(c_{12})_k(-\frac{m\pi}{r_j\alpha}u_{\theta mjk}+\frac{1}{r_j}u_{rmjk})\\
&+(c_{13})_k\sum_{n=1}^{N_z}A_{kn}^{z}u_{zmjn}=0,\\
&\sum_{n=1}^{N_r}A_{jn}^{r}u_{\theta mnk}+\frac{m\pi}{\alpha}u_{rmjk}-u_{\theta mjk}=0,\\
&\sum_{n=1}^{N_z}A_{kn}^{z}u_{rmjn}+\sum_{n=1}^{N_r}A_{jn}^{r}u_{zmnk}=0
\end{aligned}\tag{29c}$$

In the above equations $k = 2,\ldots, N_z - 1$; also $j = 1$ at $r = b$ and $j = N_r$ at $r = a$.

In order to carry out the eigenvalue analysis, the domain and boundary degrees of freedom are separated and in vector forms they are denoted as {d} and {b}, respectively. Based on this definition, the discretized form of the equilibrium equations and the related boundary conditions take the following forms,

Equations of motion (24-26)

$$\left[\left[K_{db}\right]\left[K_{dd}\right]\right]\begin{Bmatrix}\{b\}\\ \{d\}\end{Bmatrix}-\omega^2\left[M\right]\{d\}=\{0\}\tag{30}$$

Boundary conditions (27, 28) and (29.1-3)

$$\left[K_{bd}\right]\{d\}+\left[K_{bb}\right]\{b\}=\{0\} \tag{31}$$

Eliminating the boundary degrees of freedom in Eq. (30) using Eq. (31), this equation become

$$\left(\left[K\right]-\omega^2\left[M\right]\{d\}\right)=\{0\} \tag{32}$$

where $[K] = [K_{dd}] - [K_{db}][K_{bb}]^{-1}[K_{bd}]$. The above eigenvalue system of equations can be solved to find the natural frequencies and mode shapes of the plates.

5. Numerical results and discussion

In this section, the convergence behavior and accuracy of the method in evaluating the non-dimensional natural frequencies of isotropic and FG annular sector plates with

Table 3 Comparison of fundamental frequency parameter $\left(\Omega=\omega a^2\sqrt{\rho h/D}\right)$ for flexural vibration of annular sector plates with two straight edges simply supported for $b/a = 0.5$

α (deg)	h/a	Theories	C-C	F-C	F-S
195	0.01	McGee *et al*. (1995)	90.0837	21.4263	10.8761
		Zhou *et al*. (2009)	90.1125	21.4074	10.8522
		Present ($N_r = N_z = 9$)	90.1102	21.4065	10.8513
		Present ($N_r = N_z = 13$)	90.1124	21.4075	10.8520
		Present ($N_r = N_z = 17$)	90.1122	21.4076	10.8525
		Present ($N_r = N_z = 19$)	90.1123	21.4076	10.8524
	0.2	McGee *et al*. (1995)	70.8090	19.9986	10.2268
		Zhou *et al*. (2009)	71.9146	20.0967	10.2386
		Present ($N_r = N_z = 9$)	71.9115	20.0954	10.2392
		Present ($N_r = N_z = 13$)	71.9142	20.0964	10.2380
		Present ($N_r = N_z = 17$)	71.9143	20.0968	10.2385
		Present ($N_r = N_z = 19$)	71.9143	20.0968	10.2384
	0.4	McGee *et al*. (1995)	48.6618	17.5822	9.3661
		Zhou *et al*. (2009)	50.0059	17.7636	9.3961
		Present ($N_r = N_z = 9$)	50.0045	17.7653	9.3945
		Present ($N_r = N_z = 13$)	50.0059	17.7641	9.3958
		Present ($N_r = N_z = 17$)	50.0056	17.7638	9.3961
		Present ($N_r = N_z = 19$)	50.0056	17.7638	9.3962
210	0.01	McGee *et al*. (1995)	89.9678	20.9496	10.2631
		Zhou *et al*. (2009)	90.0265	20.9368	10.2418
		Present ($N_r = N_z = 9$)	90.0253	20.9347	10.2399
		Present ($N_r = N_z = 13$)	90.0260	20.9363	10.2410
		Present ($N_r = N_z = 17$)	90.0263	20.9369	10.2416
		Present ($N_r = N_z = 19$)	90.0264	20.9369	10.2416
	0.2	McGee *et al*. (1995)	70.7344	19.6097	9.6643
		Zhou *et al*. (2009)	71.8406	19.7064	9.6751
		Present ($N_r = N_z = 9$)	71.8420	19.7040	9.6733
		Present ($N_r = N_z = 13$)	71.8401	19.7059	9.6745
		Present ($N_r = N_z = 17$)	71.8407	19.7063	9.6751
		Present ($N_r = N_z = 19$)	71.8406	19.7063	9.6752
	0.4	McGee *et al*. (1995)	48.6117	17.2943	8.8769
		Zhou *et al*. (2009)	49.9566	17.4733	8.9043
		Present ($N_r = N_z = 9$)	49.9535	17.4714	8.9026
		Present ($N_r = N_z = 13$)	49.9555	17.4725	8.9035
		Present ($N_r = N_z = 17$)	49.9563	17.4736	8.9041
		Present ($N_r = N_z = 19$)	49.9564	17.4735	8.9041

Table 3 Continued

α (deg)	h/a	Theories	C-C	F-C	F-S
270	0.01	McGee *et al*. (1995)	89.6828	19.7282	8.5788
		Zhou *et al*. (2009)	89.7655	19.7258	8.5635
		Present ($N_r = N_z = 9$)	89.7634	19.7219	8.5611
		Present ($N_r = N_z = 13$)	89.7642	19.7245	8.5623
		Present ($N_r = N_z = 17$)	89.7651	19.7257	8.5630
		Present ($N_r = N_z = 19$)	89.7653	19.7259	8.5633
	0.2	McGee *et al*. (1995)	70.5516	18.6218	8.1304
		Zhou *et al*. (2009)	71.6588	18.7149	8.1386
		Present ($N_r = N_z = 9$)	71.6551	18.7117	8.1365
		Present ($N_r = N_z = 13$)	71.6575	18.7139	8.1377
		Present ($N_r = N_z = 17$)	71.6584	18.7150	8.1386
		Present ($N_r = N_z = 19$)	71.6586	18.7150	8.1387
	0.4	McGee *et al*. (1995)	48.4901	16.5657	7.5461
		Zhou *et al*. (2009)	49.8361	16.7386	7.5670
		Present ($N_r = N_z = 9$)	49.8341	16.7370	7.5650
		Present ($N_r = N_z = 13$)	49.8351	16.7382	7.5664
		Present ($N_r = N_z = 17$)	90.0837	21.4263	10.8761
		Present ($N_r = N_z = 19$)	90.1125	21.4074	10.8522
360	0.01	McGee *et al*. (1995)	90.1102	21.4065	10.8513
		Zhou *et al*. (2009)	90.1124	21.4075	10.8520
		Present ($N_r = N_z = 9$)	90.1122	21.4076	10.8525
		Present ($N_r = N_z = 13$)	90.1123	21.4076	10.8524
		Present ($N_r = N_z = 17$)	70.8090	19.9986	10.2268
		Present ($N_r = N_z = 19$)	71.9146	20.0967	10.2386
	0.2	McGee *et al*. (1995)	71.9115	20.0954	10.2392
		Zhou *et al*. (2009)	71.9142	20.0964	10.2380
		Present ($N_r = N_z = 9$)	71.9143	20.0968	10.2385
		Present ($N_r = N_z = 13$)	71.9143	20.0968	10.2384
		Present ($N_r = N_z = 17$)	48.6618	17.5822	9.3661
		Present ($N_r = N_z = 19$)	50.0059	17.7636	9.3961
	0.4	McGee *et al*. (1995)	50.0045	17.7653	9.3945
		Zhou *et al*. (2009)	50.0059	17.7641	9.3958
		Present ($N_r = N_z = 9$)	50.0056	17.7638	9.3961
		Present ($N_r = N_z = 13$)	50.0056	17.7638	9.3962
		Present ($N_r = N_z = 17$)	89.9678	20.9496	10.2631
		Present ($N_r = N_z = 19$)	90.0265	20.9368	10.2418

different set of boundary conditions along the circular edges are investigated.

McGee *et al*. (1995) provided the exact results for sector plates with a re-entrant corner, based on the Mindlin plate theory. As a first example, the comparative studies of the fundamental frequency parameters are given in Table 3. It is seen from Table 3 that for thin plates (h/a = 0.01) there is an excellent agreement between the present 3-D solutions and the classical solutions. For moderately thick plates (h/a = 0.2) the present 3-D solutions also agree quite well with the Mindlin solutions. For very thick plates (h/a = 0.4) the discrepancies increase, particularly for c-c plates. It is found that only nineteen DQ grid points in each direction (r and z) can yield accurate results. The same problem has been analyzed by Zhou *et al*. (2009). It is obvious that the error of the Mindlin plate theory increases with the increase of the plate thickness, especially for very thick plates ($h/a \geq$ 0.4). The two-dimensional theories, such as the classical plate theory, the first and the higher order shear deformation plate theories neglect transverse normal deformations, and generally assume that a plane stress state of deformation prevails in the plate. These assumptions may be appropriate

Table 4 The lowest non-dimensional frequency parameter $\left(\Omega = \omega h\sqrt{\rho/C_{11}}\right)$ for FGMs annular sector plates having clamped ($r = b$) and clamped ($r = a$) conditions

α (deg)	h/a	b/a	m (circumferential wavenumber)		λ				
					1	2	3	4	5
195	0.1	0.1	1	Nie and Zhong (2008)	0.0663	0.0622	0.0566	0.0505	0.0446
				Present ($N_r = N_z = 9$)	0.0651	0.0611	0.0553	0.0497	0.0432
				Present ($N_r = N_z = 13$)	0.0661	0.062	0.0561	0.0502	0.0440
				Present ($N_r = N_z = 17$)	0.0664	0.0622	0.0564	0.0505	0.0444
				Present ($N_r = N_z = 19$)	0.0664	0.0623	0.0564	0.0505	0.0445
			2	Nie and Zhong (2008)	0.0795	0.0746	0.0677	0.0603	0.0531
				Present ($N_r = N_z = 9$)	0.0781	0.0712	0.0666	0.0589	0.0519
				Present ($N_r = N_z = 13$)	0.0791	0.0743	0.0677	0.0601	0.0528
				Present ($N_r = N_z = 17$)	0.0793	0.0746	0.0679	0.0604	0.0530
				Present ($N_r = N_z = 19$)	0.0793	0.0747	0.0679	0.0603	0.0530
		0.3	1	Nie and Zhong (2008)	0.1041	0.0980	0.0895	0.0801	0.0710
				Present ($N_r = N_z = 9$)	0.1049	0.0968	0.0888	0.0789	0.0721
				Present ($N_r = N_z = 13$)	0.1041	0.0981	0.0896	0.0801	0.0712
				Present ($N_r = N_z = 17$)	0.1039	0.0979	0.0898	0.0799	0.0710
				Present ($N_r = N_z = 19$)	0.1039	0.0979	0.0897	0.0800	0.0710
			2	Nie and Zhong (2008)	0.1104	0.1039	0.0948	0.0849	0.0753
				Present ($N_r = N_z = 9$)	0.1094	0.1030	0.0933	0.0839	0.0741
				Present ($N_r = N_z = 13$)	0.1103	0.1038	0.0946	0.0845	0.0755
				Present ($N_r = N_z = 17$)	0.1106	0.1040	0.0950	0.0850	0.0751
				Present ($N_r = N_z = 19$)	0.1105	0.1039	0.0950	0.0850	0.0752
	0.3	0.1	1	Nie and Zhong (2008)	0.4040	0.3862	0.3611	0.3329	0.3046
				Present ($N_r = N_z = 9$)	0.4026	0.3842	0.3593	0.3314	0.3035
				Present ($N_r = N_z = 13$)	0.4038	0.3853	0.3604	0.3322	0.3045
				Present ($N_r = N_z = 17$)	0.4041	0.3863	0.3609	0.3326	0.3047
				Present ($N_r = N_z = 19$)	0.4041	0.3863	0.3610	0.3327	0.3048
			2	Nie and Zhong (2008)	0.5013	0.4781	0.4455	0.4091	0.3730
				Present ($N_r = N_z = 9$)	0.5001	0.4768	0.4438	0.4081	0.3719
				Present ($N_r = N_z = 13$)	0.5008	0.4784	0.4449	0.4090	0.3727
				Present ($N_r = N_z = 17$)	0.5011	0.4780	0.4453	0.4092	0.3730
				Present ($N_r = N_z = 19$)	0.5011	0.4779	0.4455	0.4092	0.3729
		0.3	1	Nie and Zhong (2008)	0.6077	0.5840	0.5504	0.5125	0.4744
				Present ($N_r = N_z = 9$)	0.6061	0.5852	0.5494	0.5120	0.4761
				Present ($N_r = N_z = 13$)	0.6075	0.5846	0.5500	0.5127	0.4754
				Present ($N_r = N_z = 17$)	0.6079	0.5843	0.5505	0.5124	0.4748
				Present ($N_r = N_z = 19$)	0.6079	0.5842	0.5505	0.5124	0.4746
			2	Nie and Zhong (2008)	0.6077	0.5840	0.5504	0.5125	0.4744
				Present ($N_r = N_z = 9$)	0.6061	0.5852	0.5494	0.5120	0.4761
				Present ($N_r = N_z = 13$)	0.6075	0.5846	0.5500	0.5127	0.4754
				Present ($N_r = N_z = 17$)	0.6079	0.5843	0.5505	0.5124	0.4748
				Present ($N_r = N_z = 19$)	0.6079	0.5842	0.5505	0.5124	0.4746

for thin plates but do not give good results for thick plates. It is seen from Table 3 that the maximum differences between the 3-D solutions and the Mindlin solutions occur at the clamped-clamped plates. A numerical value of $N_r = N_z = 19$ is used for the next studies. As the second example, the convergence behavior and accuracy of the method for

Table 4 Continued

α (deg)	h/a	b/a	m (circumferential wavenumber)		λ				
					1	2	3	4	5
				Nie and Zhong (2008)	0.0659	0.0619	0.0563	0.0502	0.0443
				Present ($N_r = N_z = 9$)	0.0651	0.0603	0.0550	0.0509	0.0451
			1	Present ($N_r = N_z = 13$)	0.0665	0.0617	0.0555	0.0504	0.0440
				Present ($N_r = N_z = 17$)	0.0661	0.0621	0.0560	0.0501	0.0445
		0.1		Present ($N_r = N_z = 19$)	0.0660	0.0621	0.0561	0.0501	0.0444
				Nie and Zhong (2008)	0.0766	0.0719	0.0653	0.0581	0.0512
				Present ($N_r = N_z = 9$)	0.0751	0.0705	0.0641	0.0573	0.0500
			2	Present ($N_r = N_z = 13$)	0.0760	0.0717	0.0650	0.0581	0.0508
				Present ($N_r = N_z = 17$)	0.0765	0.0720	0.0655	0.0583	0.0511
	0.1			Present ($N_r = N_z = 19$)	0.0765	0.0721	0.0654	0.0583	0.0510
				Nie and Zhong (2008)	0.1039	0.0978	0.0892	0.0799	0.0708
				Present ($N_r = N_z = 9$)	0.1025	0.0969	0.0883	0.0787	0.0681
			1	Present ($N_r = N_z = 13$)	0.1033	0.0979	0.0892	0.0807	0.0693
				Present ($N_r = N_z = 17$)	0.1038	0.0976	0.0895	0.0801	0.0701
		0.3		Present ($N_r = N_z = 19$)	0.1037	0.0977	0.0895	0.0800	0.0706
				Nie and Zhong (2008)	0.1090	0.1027	0.0937	0.0839	0.0744
				Present ($N_r = N_z = 9$)	0.1099	0.1039	0.0944	0.0849	0.0757
			2	Present ($N_r = N_z = 13$)	0.1095	0.1033	0.0939	0.0842	0.0749
				Present ($N_r = N_z = 17$)	0.1091	0.1028	0.0936	0.0839	0.0744
				Present ($N_r = N_z = 19$)	0.1092	0.1029	0.0935	0.0839	0.0745
210				Nie and Zhong (2008)	0.4002	0.3827	0.3580	0.3302	0.3023
				Present ($N_r = N_z = 9$)	0.4018	0.3815	0.3598	0.3318	0.3003
			1	Present ($N_r = N_z = 13$)	0.4007	0.3824	0.3587	0.3308	0.3018
				Present ($N_r = N_z = 17$)	0.4001	0.3829	0.3581	0.3303	0.3023
		0.1		Present ($N_r = N_z = 19$)	0.4000	0.3829	0.3582	0.3304	0.3023
				Nie and Zhong (2008)	0.4832	0.4608	0.4294	0.3943	0.3594
				Present ($N_r = N_z = 9$)	0.4813	0.4622	0.4277	0.3931	0.3577
			2	Present ($N_r = N_z = 13$)	0.4826	0.4611	0.4288	0.3940	0.3587
				Present ($N_r = N_z = 17$)	0.4834	0.4605	0.4295	0.3944	0.3594
	0.3			Present ($N_r = N_z = 19$)	0.4833	0.4606	0.4296	0.3944	0.3595
				Nie and Zhong (2008)	0.5630	0.5421	0.5123	0.4784	0.4439
				Present ($N_r = N_z = 9$)	0.5618	0.5404	0.5105	0.4799	0.4424
			1	Present ($N_r = N_z = 13$)	0.5629	0.5415	0.5117	0.4790	0.4434
				Present ($N_r = N_z = 17$)	0.5633	0.5422	0.5121	0.4785	0.4439
		0.3		Present ($N_r = N_z = 19$)	0.5633	0.5421	0.5121	0.4784	0.4440
				Nie and Zhong (2008)	0.5990	0.5756	0.5428	0.5056	0.4682
				Present ($N_r = N_z = 9$)	0.5977	0.5771	0.5441	0.5041	0.4702
			2	Present ($N_r = N_z = 13$)	0.5984	0.5760	0.5433	0.5050	0.4690
				Present ($N_r = N_z = 17$)	0.5990	0.5756	0.5429	0.5055	0.4683
				Present ($N_r = N_z = 19$)	0.5991	0.5755	0.5429	0.5057	0.4683

lowest non-dimensional frequency parameter ($\varpi = \omega h\sqrt{\rho/C_{11}}$) of thick FG annular sector plates with clamped-clamped boundary condition at circular edges are studied in Table 4. The results are compared with those of the three-dimensional elasticity solutions of Nie and Zhong (2008) which were obtained using the State space method (S.S.M). It is assumed that the material properties vary exponentially$\left(c_{ij}(z) = c_{ij}^{M} e^{\left(\frac{\lambda z}{h}\right)},\ \rho(z) = \rho^{M} e^{\left(\frac{\lambda z}{h}\right)}\right)$ through

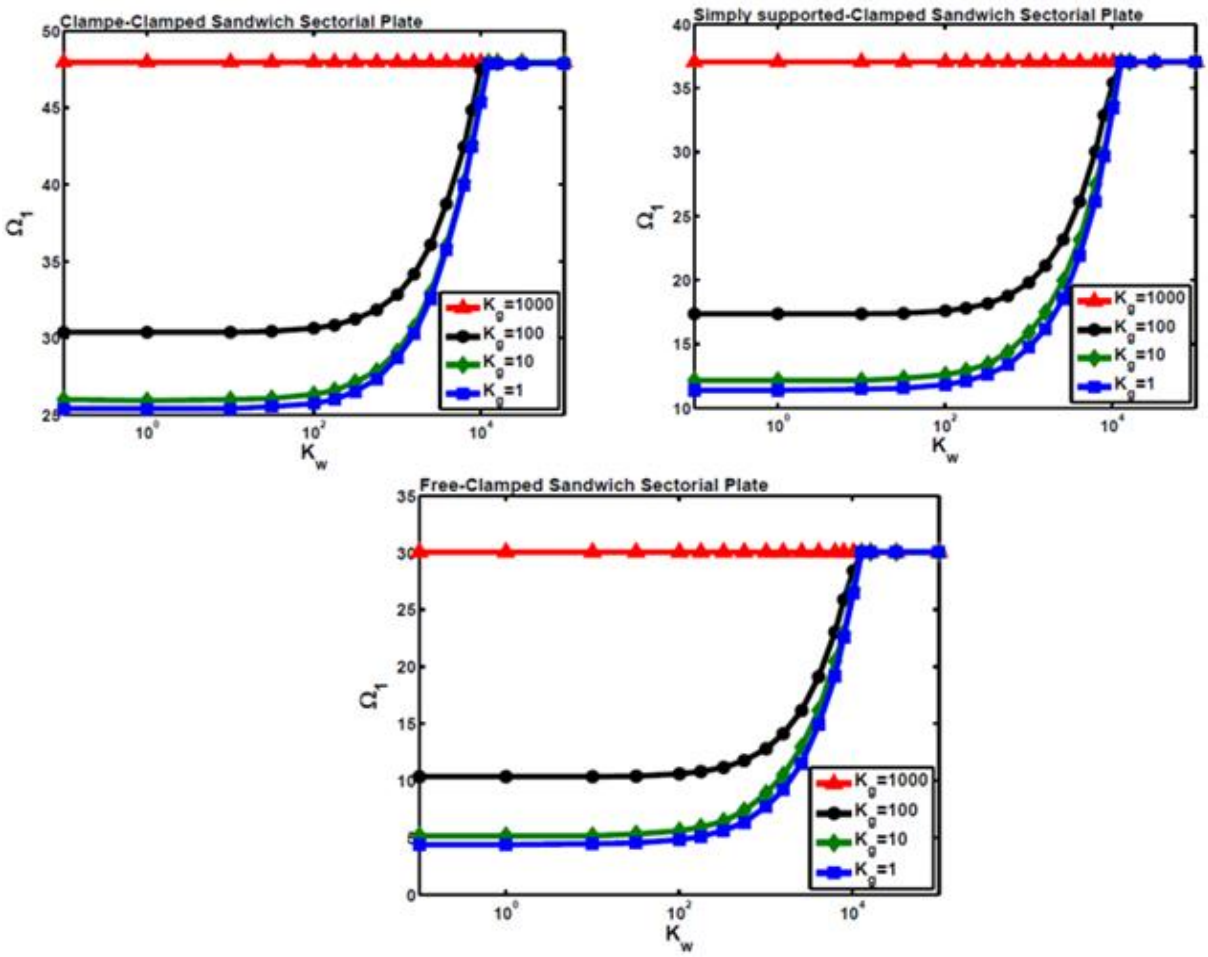

Fig. 3 Variation of the first non-dimensional natural frequency parameter of sandwich annular sector plate with Winkler and different shearing layer elastic coefficient for different types of boundary conditions (h/a = 0.2, V_{CN}^{*} = 0.28, α = 90°, w = 0, FG-V)

the thickness of the plate. Superscripts M denote the material properties of the bottom surface of the plate, λ is the material property graded index. One can see that an excellent agreement exists between the converged results of the presented approach and the other one. In this section, we characterize the response of FG sector plate considering the effects of waviness and aspect ratio. The non-dimensional natural frequency, Winkler and shearing layer elastic coefficients are assumed as follows (Tahouneh 2017)

$$\Omega = \omega a^2 \sqrt{\rho_i h / D_i} \quad , \quad D_i = E_i h^3 / 12(1-\upsilon_i^2) \tag{33}$$

where ρ_i, E_i and υ_i are mechanical properties of CNT.

$$K_g = k_g a^2 / D_i \quad , \quad K_w = k_w a^4 / D_i \tag{34}$$

The effects of variation of the Winkler elastic coefficient on the first non-dimensional natural frequency parameters of FG sandwich annular sector plate and for different values of shearing layer elastic coefficient and sets of boundary conditions are shown in Fig. 3. It is clear that in all cases, with increasing the elastic coefficients of the foundation, the frequency parameters increase to some limit values. It is observed for the large values of Winkler elastic coefficient, the shearing layer elastic coefficient has less effect and the results become independent of it.

The influence of shearing layer elastic coefficient on the first non-dimensional natural frequencies for Clamped-Clamped boundary condition is shown in Fig. 4. One can see that the Winkler elastic coefficient has little effect on the non-dimensional natural frequencies at different values of shearing layer elastic coefficient. It should be noted that this behavior is also observed at other types of boundary conditions, but, for the sale of brevity, they are not shown here.

Wave number, m, is calculated and plotted in Fig. 5. This figure is representing the five different FG material distributions (FG-V, FG-X, FG-Λ, FG-O and UD). The results for UD sectorial plate are included for direct comparison. It can be noticed that the plate of FG-V material distribution has highest, while the plates of FG-X and FG-O material distribution are nearly the same and the UD plate has the lowest normalized natural frequency among the five.

The effect of CNT aspect ratio is depicted in Fig. 6. This figure illustrates frequency parameters of Clamped-Clamped, Simply supported-Clamped and Free-Clamped

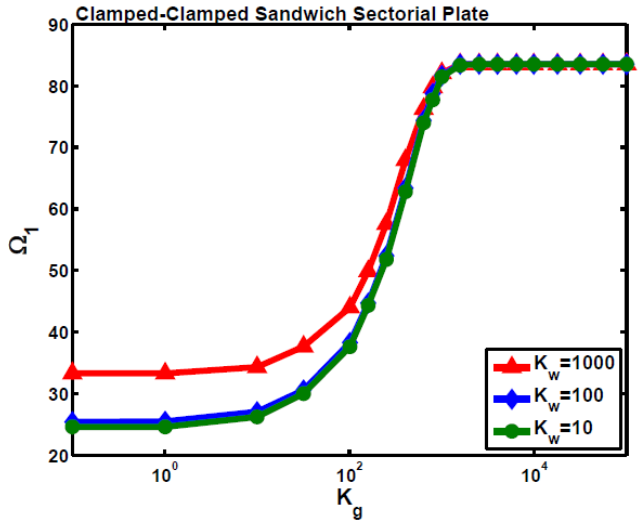

Fig. 4 Geometry of the sandwich annular sector plate on an elastic foundation conditions (h/a = 0.2, V_{CN}^* = 0.28, α = 90°, w = 0, AR = 1000, FG-V)

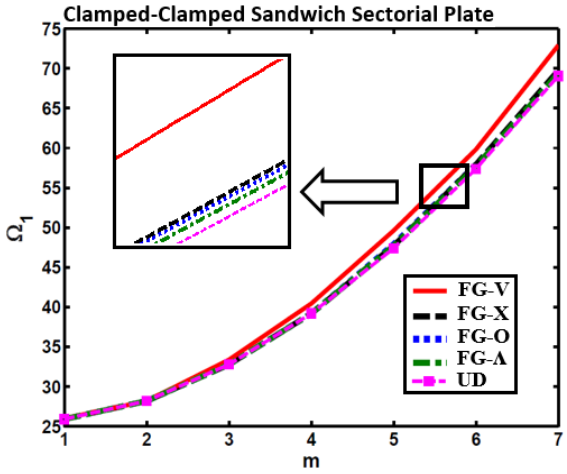

Fig. 5 The effect of the circumferential wave number (m) on the normalized natural frequency for Clamped-Clamped sandwich sectorial plates on elastic foundations (h/a = 0.2, V_{CN}^* = 0.28, α = 90°, w = 0, AR = 1000, K_g = K_w = 10)

sandwich sectorial plates for different amounts of V_{CN}^*, including 0.12, 0.17 and 0.28. This figure reveals that increasing of CNT aspect ratio leads to a little increases frequency parameters for different types of boundary conditions.

Fig. 7 shows the effect of volume fraction of CNTs on

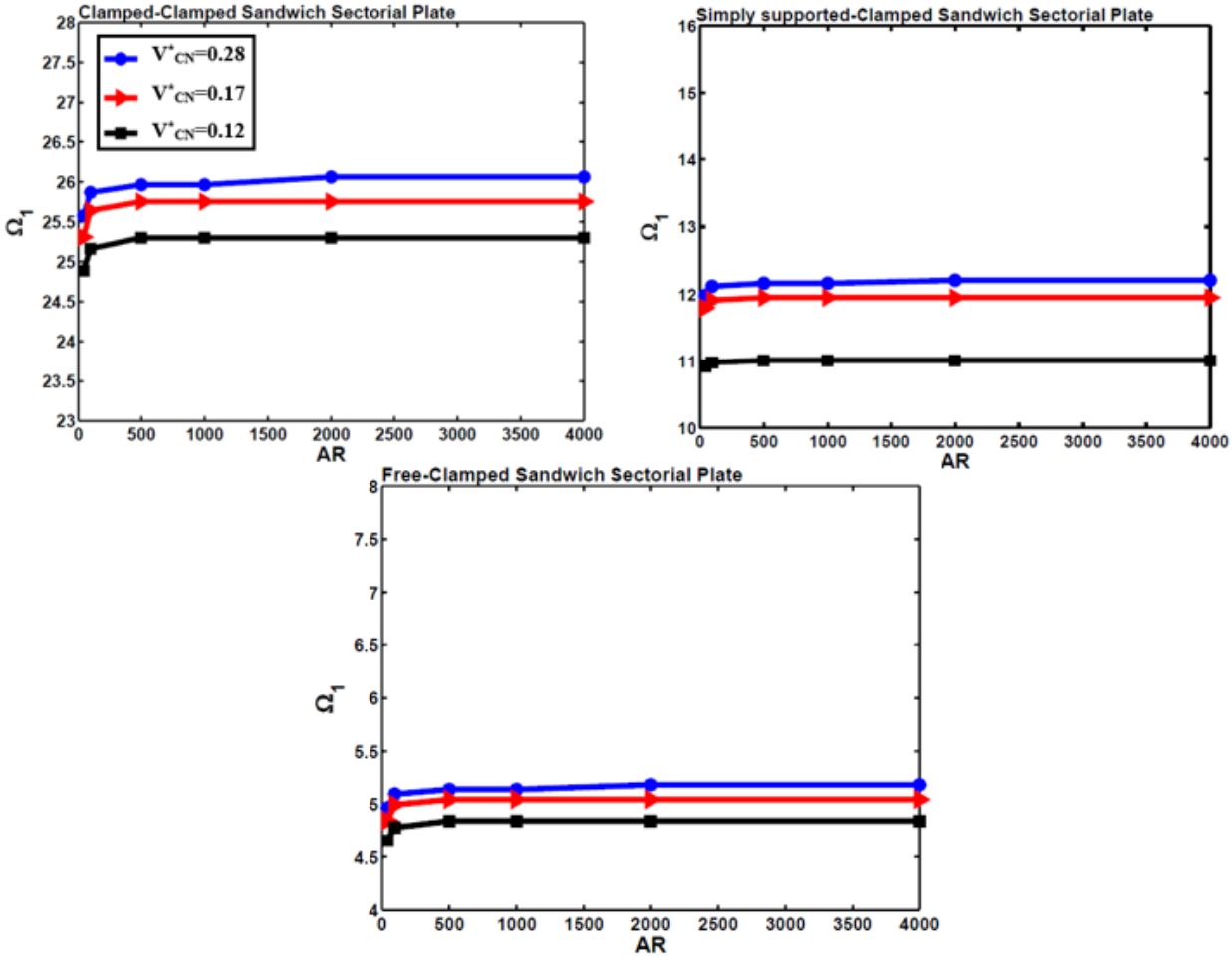

Fig. 6 The variation of frequency parameters versus aspect ratio (AR) for FG-V sandwich sectorial plates (h/a = 0.2, V_{CN}^* = 0.28, α = 90°, w = 0)

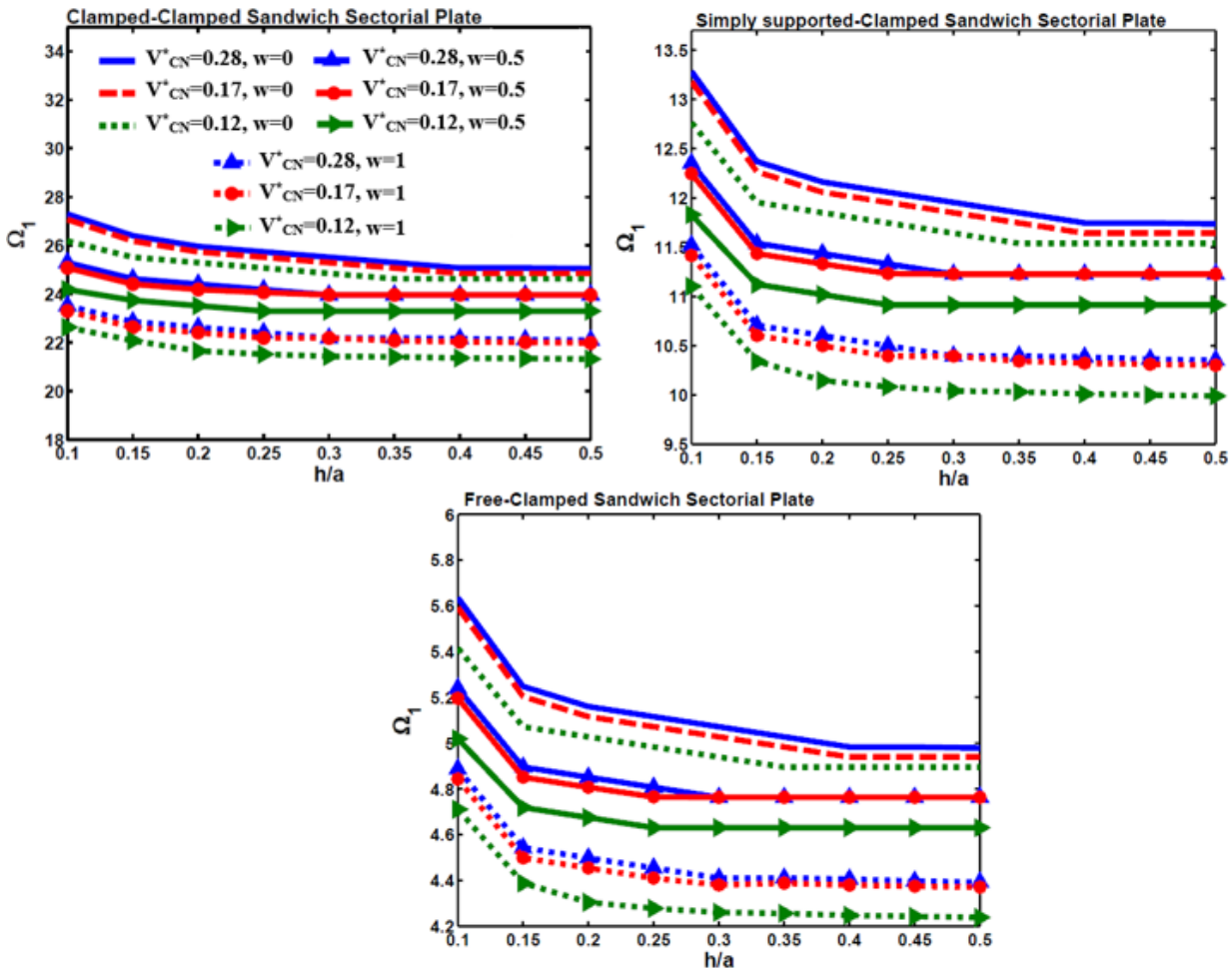

Fig. 7 The effect of h/a on the normalized natural frequency of sectorial plates with different types of boundary conditions at circular edges resting on elastic foundations ($K_w = K_q = 10$, AR = 1000, $h/a = 0.2$, $\alpha = 90°$, FG-V)

the normalized natural frequencies of sandwich sectorial plates for different types of boundary conditions at circular edges. It is observed that the normalized natural frequency of the plates increases with increasing of V_{CN}^{*}. Results show that by increasing the values of waviness index (w), normalized natural frequency of sectorial plate decreases, and the straight CNT gives highest frequency.

It also shows that the non-dimensional natural frequency decreases with the increase of h/a ratio and then remains almost unaltered for great amount of thickness-to-outer radius ratio, h/a.

6. Conclusions

In this research work, free vibration of continuous grading sandwich sectorial plates on a two-parameter elastic foundation is investigated. The elastic foundation is considered as a Pasternak model with adding a shear layer to the Winkler model. This study is carried out based on the three-dimensional theory of elasticity. The aim of this study is to fill this apparent gap in this area by investigating the effects of CNTs waviness and aspect ratio on vibrational behavior of FG sandwich annular sector plates on elastic foundations. Five linear types of distributions of CNTs are considered; uniform and four kinds of FG distributions along the thickness of face sheets and the effects of CNT volume fraction, aspect ratio and waviness and also Pasternak's elastic foundation coefficients, sandwich plate thickness, face sheets thickness are investigated on the free vibrational behavior of sandwich plates with wavy CNT-reinforced face sheets. The material properties estimated through the extended rule of mixture. Micromechanics equations cannot capture the scale difference between the nano- and micro- levels. To overcome this difficulty, the efficiency parameter is defined. In this research work, 2-D differential quadrature method is used to study different types of boundary conditions at circular edges including Free, Clamped and Simply supported. Using 2-D differential quadrature method in the r- and z-directions, allows one to deal with FG plates with arbitrary thickness distribution of material properties and also to implement the effects of the elastic foundations as a boundary condition on the lower surface of the plate efficiently and in an exact manner. The fast rate of convergence and accuracy of the method are investigated through the different solved examples. From this study some conclusions can be made as following:

- It is shown that the variation of Winkler elastic

coefficient has little effect on the non-dimensional natural frequencies at different values of shearing layer elastic coefficient. It is clear that in all cases, with increasing the shearing layer elastic coefficient of the foundation, the frequency parameters increase to some limit values.

- It is shown that for the large values of shearing layer elastic coefficient; the results become independent of it. It is also shown that with increasing the elastic coefficients of the foundation, the frequency parameters increase to some limit values.
- The waviness can significantly reduce the stiffening effect of the nanotubes.
- By increasing the values of waviness index, normalized natural frequency of sectorial plate decreases, and the straight CNT gives highest frequency.
- Normalized natural frequency of sectorial plate that reinforced by long and short CNTs is compared for the same waviness index; biggest normalized natural frequency is found in the case of long CNT with reference to short one.
- It also shows that the non-dimensional natural frequency decreases with the increase of h/a ratio and then remains almost unaltered for great amount of thickness-to-outer radius ratio, h/a.
- Results reveal that increasing of CNT aspect ratio leads to a little increases frequency parameters.
- In this study five different FG material distributions (FG-V, FG-X, FG-Λ, FG-O and UD) are considered. The results for UD sectorial plate are included for direct comparison. It can be noticed that the plate of FG-V material distribution has highest, while the plates of FG-X and FG-O material distribution are nearly the same and the UD plate has the lowest normalized natural frequency among the five.

References

Affdl Halpin, J.C. and Kardos, J.L. (1976), "The Halpin-Tsai equations: A review", *Polym. Eng. Sci.*, **16**(5), 344-352.

Arefi, M. (2015), "Elastic solution of a curved beam made of functionally graded materials with different cross sections', *Steel Compos. Struct., Int. J.*, **18**(3), 659-672.

Barka, M., Benrahou, K.H., Bakora, A. and Tounsi, A. (2016), "Thermal post-buckling behavior of imperfect temperature-dependent sandwich FGM plates resting on Pasternak elastic foundation", *Steel Compos. Struct., Int. J.*, **22**(1), 91-112.

Bennai, R., Ait Atmane, H. and Tounsi, A. (2015), "A new higher-order shear and normal deformation theory for functionally graded sandwich beams", *Steel Compos. Struct., Int. J.*, **19**(3), 521-546.

Bert, C.W. and Malik, M. (1996), "Differential quadrature method in computational mechanics: a review", *Appl. Mech. Rev.*, **49**, 1-27.

Bouchafa, A., Bouiadjra, M.B., Houari, M.S.A. and Tounsi, A. (2015), "Thermal stresses and deflections of functionally graded sandwich plates using a new refined hyperbolic shear deformation theory", *Steel Compos. Struct., Int. J.*, **18**(6), 1493-1515.

Bouguenina, O., Belakhdar, K., Tounsi, A. and Bedia, E.A.A. (2015), "Numerical analysis of FGM plates with variable thickness subjected to thermal buckling", *Steel Compos. Struct., Int. J.*, **19**(3), 679-695.

Brischetto, S. and Tornabene, F. (2018), "Advanced GDQ models and 3D stress recovery in multilayered plates, spherical and double-curved panels subjected to transverse shear loads", *Compos. Part B*, **146**, 244-269.

Chen, C.S., Liu, F.H. and Chen, W.R. (2017), "vibration and stability of initially stressed sandwich plates with FGM face sheets in thermal environments", *Steel Compos. Struct., Int. J.*, **23**(3), 251-261.

Fantuzzi, N., Tornabene, F., Bacciocchi, M. and Dimitri, R. (2017), "Free vibration analysis of arbitrarily shaped Functionally Graded Carbon Nanotube-reinforced plates", *Compos. Part B*, **115**, 384-408.

Farsadi, M., Ö chsner, A. and Rahmandoust, M. (2013), "Numerical investigation of composite materials reinforced with waved carbon nanotubes", *J. Compos. Mater.*, **47**(11), 1425-1434.

Fidelus, J.D., Wiesel, E., Gojny, F.H., Schulte, K. and Wagner, H.D. (2005), "Thermo-mechanical properties of randomly oriented carbon/epoxy nanocomposites", *Compos. Part A*, **36**, 1555-1561.

Finot, M. and Suresh, S. (1996), "Small and large deformation of thick and thin-film multilayers: effect of layer geometry, plasticity and compositional gradients", *J. Mech. Phys. Solids*, **44**(5), 683-721.

Ghavamian, A., Rahmandoust, M. and Öchsner, A. (2012), 62, "A numerical evaluation of the influence of defects on the elastic modulus of single and multi-walled carbon nanotubes", *Comput. Mater. Sci.*, **62**, 110-116.

Gojny, F.H., Wichmann, M.H.G., Fiedler, B. and Schulte, K. (2005), "Influence of different carbon nanotubes on the mechanical properties of epoxy matrix composites-A comparative study", *Compos. Sci. Technol.*, **65**, 2300-2313.

Halpin, J.C. and Tsai, S.W. (1969), "Effects of environmental factors on composite materials", *AFML-TR*-67-423.

Houmat, A. (2001), "A sector Fourier p-element applied to free vibration analysis of sectorial plates", *J. Sound Vib.*, **243**(2), 269-282.

Kamarian, S., Yas, M.H. and Pourasghar, A. (2013), "Free vibration analysis of three-parameter functionally graded material sandwich plates resting on Pasternak foundations", *J. Sandw. Struct. Mater.*, **15**(3), 292-308.

Kamarian, S., Sadighi, M. and Shakeri, M. (2014), "Free vibration response of sandwich cylindrical shells with functionally graded material face sheets resting on Pasternak foundation", *J. Sandw. Struct. Mater.*, **16**(5), 511-533.

Kamarian, S., Shakeri, M., Yas, M.H., Bodaghi, M. and Pourasghar, A. (2015), "Free vibration analysis of functionally graded nanocomposite sandwich beams resting on Pasternak foundation by considering the agglomeration effect of CNTs", *J. Sandw. Struct. Mater.*, 1-31.

Kamarian, S., Salim, M., Dimitri, R. and Tornabene, F. (2016), "Free vibration analysis of conical shells reinforced with agglomerated Carbon Nanotubes", *Int. J. Mech. Sci.*, **1**(108-109), 157-165.

Kim, C.S. and Dickinson, S.M. (1989), "On the free, transverse vibration of annular and circular, thin, sectorial plates subjected to certain complicating effects", *J. Sound Vib.*, **134**(3), 407-421.

Koizumi, M. (1993), "The concept of FGM", *Ceram. Trans. Funct. Grad. Mater.*, **34**, 3-10.

Leissa, A.W., McGee, O.G. and Huang, C.S. (1993), "Vibrations of sectorial plates having corner stress singularities", *J. Appl. Mech. Transactions of the ASME*, **60**(1), 134-140.

Liew, K.M. and Lam, K.Y. (1993), "On the use of 2-d orthogonal polynomials in the Rayleigh-Ritz method for flexural vibration of annular sector plates of arbitrary shape", *Int. J. Mech. Sci.*,

35(2), 129-139.
Liew, K.M. and Liu, F.L. (2000), "Differential quadrature method for vibration analysis of shear deformable annular sector plates", *J. Sound Vib.*, **230**(2), 335-356.
Marin, M. (1994), "The Lagrange identity method in thermoelasticity of bodies with microstructure", *Int. J. Eng. Sci.*, **32**(8), 1229-1240.
Marin, M. (2008), "Weak Solutions in Elasticity of Dipolar Porous Materials", *Math. Prob. Eng.*, **2008**(1-8), Art. No. 158908.
Marin, M. (2016), "An approach of a heat-flux dependent theory for micropolar porous media", *Meccanica*, **51**(5), 1127-1133.
Marin, M. and Baleanu, D. (2016), "On vibrations in thermoelasticity without energy dissipation for micropolar bodies", *Bound. Value Probl.*, **111**, 1-19.
Marin, M., Agarwal, R.P., Mahmoud, S.R. (2013), "Modeling a microstretch thermo-elastic body with two temperatures", *Abstract and Applied Analysis*, **2013**(1-7), Art. ID 583464.
Martone, A., Faiella, G., Antonucci, V., Giordano, M. and Zarrelli, M. (2011), "The effect of the aspect ratio of carbon nanotubes on their effective reinforcement modulus in an epoxy matrix", *Compos. Sci. Technol.*, **71**(8), 1117-1123.
McGee, O.G., Huang, C.S. and Leissa, A.W. (1995), "Comprehensive exact solutions for free vibrations of thick annular sectorial plates with simply supported radial edges", *Int. J. Mech. Sci.*, **37**(5), 537-566.
Montazeri, A., Javadpour, J., Khavandi, A., Tcharkhtchi, A. and Mohajeri, A. (2010), "Mechanical properties of multi-walled carbon nanotube/epoxy composites", *Mater. Des.*, **31**, 4202-4208.
Moradi-Dastjerdi, R., Foroutan, M., Pourasghar, A. (2013), "Dynamic analysis of functionally graded nanocomposite cylinders reinforced by carbon nanotube by a mesh-free method", *Mater. Des.*, **44**, 256-266.
Moradi-Dastjerdi, R. and Momeni-Khabisi, H. (2016), "Dynamic analysis of functionally graded nanocomposite plates reinforced by wavy carbon nanotube", *Steel Compos. Struct., Int. J.*, **22**(2).
Mukhopadhyay, M. (1979), "A semi-analytic solution for free vibration of annular sector plates", *J. Sound Vib.*, **63**(1), 87-95.
Mukhopadhyay, M. (1982), "Free vibration of annular sector plates with edges possessing different degrees of rotational restraints", *J. Sound Vib.*, **80**(2), 275-279.
Nie, G.J. and Zhong, Z. (2008), "Vibration analysis of functionally graded annular sectorial plates with simply supported radial edges", *Compos. Struct.*, **84**(2), 167-176.
Park, W.T., Han, S.C., Jung, W.Y. and Lee, W.H. (2016), "Dynamic instability analysis for S-FGM plates embedded in Pasternak elastic medium using the modified couple stress theory", *Steel Compos. Struct., Int. J.*, **22**(6), 1239-1259.
Pelletier Jacob, L. and Vel Senthil, S. (2006), "An exact solution for the steady state thermo elastic response of functionally graded orthotropic cylindrical shells", *Int. J. Solid Struct.*, **43**, 1131-1158.
Ramaiah, G.K. and Vijayakumar, K. (1974), "Natural frequencies of circumferentially truncated sector plates with simply supported straight edges", *J. Sound Vib.*, **34**(1), 53-61.
Ramakris, R. and Kunukkas, V.X. (1973), "Free vibration of annular sector plates", *J. Sound Vib.*, **30**(1), 127-129.
Reddy, J.N. (2013), *An Introduction to Continuum Mechanics*, (Second Edition), Cambridge University Press.
Seok, J.W. and Tiersten, H.F. (2004), "Free vibrations of annular sector cantilever plates part 1:out-of-plane motion", *J. Sound Vib.*, **271**(3-5), 757-772.
Sharma, A., Sharda, H.B. and Nath, Y. (2005a), "Stability and vibration of Mindlin sector plates: an analytical approach", *AIAA Journal*, **43**(5), 1109-1116.
Sharma, A., Sharda, H.B. and Nath, Y. (2005b), "Stability and vibration of thick laminated composite sector plates", *J. Sound Vib.*, **287**(1-2), 1-23.
Shen, H.S. (2009), "Nonlinear bending of functionally graded carbon nanotube reinforced composite plates in thermal environments", *Compos. Struct.*, **91**(1), 9-19.
Shen, H.S. and Zhang, C.L. (2010), "Thermal buckling and postbuckling behavior of functionally graded carbon nanotube-reinforced composite plates", *Mater. Des.*, **31**(7), 3403-3411.
Shi, D.L., Feng, X.Q., Huang, Y.Y., Hwang, K.C. and Gao, H. (2004), "The Effect of Nanotube Waviness and Agglomeration on the Elastic Property of Carbon Nanotube-Reinforced Composites", *J. Eng. Mater. Technol.*, 126(3) 250-257.
Sobhani Aragh, B., Nasrollah Barati, A.H. and Hedayati, H. (2012), "Eshelby–Mori–Tanaka approach for vibrational behavior of continuously graded carbon nanotube-reinforced cylindrical panels", *Compos. B Eng.*, **43**(4), 1943-1954.
Srinivasan, R.S. and Thiruvenkatachari, V. (1983), "Free vibration of annular sector plates by an integral equation technique", *J. Sound Vib.*, **89**(3), 425-432.
Srinivasan, R.S. and Thiruvenkatachari, V. (1986), "Free vibration analysis of laminated annular sector plates", *J. Sound Vib.*, **109**(1), 89-96.
Swaminadham, M., Danielski, J. and Mahrenholtz, O. (1984), "Free vibration analysis of annular sector plates by holographic experiments", *J. Sound Vib.*, **95**(3), 333-340.
Tahouneh, V. (2016), "Using an equivalent continuum model for 3D dynamic analysis of nanocomposite plates", *Steel Compos. Struct., Int. J.*, **20**(3), 623-649.
Tahouneh, V. (2017), "The effect of carbon nanotubes agglomeration on vibrational response of thick functionally graded sandwich plates", *Steel Compos. Struct., Int. J.*, **24**(6), 711-726.
Tornabene, F. and Brischetto, S. (2018), "3D capability of refined GDQ models for the bending analysis of composite and sandwich plates, spherical and doubly-curved shells", *Thin-Wall. Struct.*, **129**, 94-124.
Tornabene, F., Fantuzzi, N., Ubertini, F. and Viola, E. (2015), "Strong formulation finite element method based on differential quadrature: a survey", *Appl. Mech. Rev.*, **67**(2), 1-55.
Tornabene, F., Fantuzzi, N., Bacciocchi, M. and Viola, E. (2016), "Effect of agglomeration on the natural frequencies of functionally graded carbon nanotube-reinforced laminated composite doubly-curved shells", *Compos. Part B*, **89**, 187-218.
Tornabene, F., Fantuzzi, N. and Bacciocchi, M. (2017a), "Linear static response of nanocomposite plates and shells reinforced by agglomerated carbon nanotubes", *Composite Part B.*, **115**, 449-476.
Tornabene, F., Fantuzzi, N., Bacciocchi, M., Viola, E. and Reddy, J.N. (2017b), "A numerical investigation on the natural frequencies of FGM sandwich shells with variable thickness by the local generalized differential quadrature method", *Appl. Sci.*, **7**(2), 1-39.
Tornabene, F., Bacciocchi, M., Fantuzzi, N. and Reddy, J.N. (2018), "Multiscale Approach for Three-Phase CNT/Polymer/ Fiber Laminated Nanocomposite Structures", *Polym. Compos.* DOI: 10.1002/pc.24520 [In Press]
Wagner, H.D., Lourie, O. and Feldman, Y. (1997), "Stress-induced fragmentation of multiwall carbon nanotubes in a polymer matrix", *Appl. Phys. Lett.*, **72**(2), 188-190.
Weidt, D. and Figiel, L. (2015), "Effect of CNT waviness and van der Waals interaction on the nonlinear compressive behaviour of epoxy/CNT nanocomposites", *Compos. Sci. Technol.*, **115**, 52-59.
Wu, C.P. and Liu, Y.C. (2016), "A state space meshless method for the 3D analysis of FGM axisymmetric circular plates", *Steel Compos. Struct., Int. J.*, **22**(1), 161-182.
Yeh, M.K., Tai, N.H. and Liu, J.H. (2006), "Mechanical behavior of phenolic-based composites reinforced with multi-walled

carbon nanotubes", *Carbon*, **44**(1), 1-9.
Zhou, D., Lo, S.H. and Cheung, Y.K. (2009), "3-D vibration analysis of annular sector plates using the Chebyshev-Ritz method", *J. Sound Vib*., **320**(1-2), 421-437.
Zhu, X.H. and Meng, Z.Y. (1995), "Operational principle fabrication and displacement characteristics of a functionally gradient piezoelectricceramic actuator", *Sens. Actuators*, **48**(3), 169-176.

CC

Appendix

In Generalized Differential Quadrature Method (GDQM), the *n*th order partial derivative of a continuous function $f(x, z)$ with respect to x at a given point x_i can be approximated as a linear summation of weighted function values at all the discrete points in the domain of x, that is

$$\frac{\partial^n f(x_i,z)}{\partial x^n}=\sum_{k=1}^{N} c_{ik}^n f(x_{ik},z) \quad (i=1,2,...,N, n=1,2,...,N-1) \tag{1}$$

where N is the number of sampling points and c_{ij}^n is the x^i dependent weight coefficient. To determine the weighting coefficients c_{ij}^n, the Lagrange interpolation basic functions are used as the test functions, and explicit formulas for computing these weighting coefficients can be obtained as (Bert and Malik 1996)

$$c_{ij}^{(1)}=\frac{M^{(1)}(x_i)}{(x_i-x_j)M^{(1)}(x_j)}, i, j=1,2,...,N, i\neq j \tag{2}$$

where

$$M^{(1)}(x_i)=\prod_{j=1, i\neq j}^{N}(x_i-x_j) \tag{3}$$

and for higher order derivatives, one can use the following relations iteratively

$$c_{ij}^{(n)}=n(c_{ii}^{(n-1)}c_{ij}^{1}-\frac{c_{ij}^{(n-1)}}{(x_i-x_j)}), \quad i, j=1,2,...,N, \quad i\neq j, n=2,3,...,N-1 \tag{4}$$

$$c_{ii}^{(n)}=-\sum_{j=1, i\neq j}^{N} c_{ij}^{(n)} \quad i=1,2,...,N, \quad n=1,2,...,N-1 \tag{5}$$

A simple and natural choice of the grid distribution is the uniform grid-spacing rule. However, it was found that nonuniform grid-spacing yields result with better accuracy. Hence, in this work, the Chebyshev-Gauss-Lobatto quadrature points are used

$$x_i=\frac{1}{2}(1-\cos(\frac{i-1}{N-1}\pi)) \quad i=1,2,...,N \tag{6}$$